An Introduction to Quintessence

R. R. Caldwell

Department of Physics, Princeton University, Princeton, New Jersey 08544 USA

Received 7 January, 2000

There is a missing energy problem in cosmology: the total energy density of the Universe, based on a wide range of observations, is much greater than the energy density contributed by all baryons, neutrinos, photons, and dark matter. Deepening this mystery are the recent observations of type 1a supernovae which suggest that the expansion rate of the Universe is accelerating. One possible resolution is the existence of a cosmological constant which fills this energy gap. However, a logical alternative is "quintessence," a time-dependent, spatially inhomogeneous, negative pressure energy component which drives the cosmic expansion. This lecture will serve as an introduction to the quintessence cosmological scenario.

I Introduction

One of the most important challenges in cosmology is the determination of the composition of the Universe. Remarkably, recent developments suggest that most of the energy density in the Universe, beyond the dark matter, is unaccounted for or missing. Observations of a low matter density in cold dark matter (CDM) and baryons (see [1] for a review and [2] for recent results) fall short of the critical value required for spatial flatness. However, current measurements of the cosmic microwave background (CMB) anisotropy spectrum strongly support a spatially flat Universe [3], indicating a shortfall in the total energy density. To account for this "missing energy," the cosmological constant (Λ) has been proposed to fill the gap [4, 5], and also explain the accelerating expansion inferred from type 1a supernovae [6, 7]. There is another class of cosmological models, however, which fit the current data just as well and are on an equal if not stronger theoretical ground than Λ — that is, Quintessence.

Quintessence (Q) is a time-varying, spatially-inhomogeneous, negative pressure component of the cosmic fluid [8, 9]. It is distinct from Λ in that it is *dynamic*: the Q energy density and pressure vary with time and is spatially inhomogeneous. A common example of quintessence is a scalar field slowly rolling down a potential, similar to the inflaton in inflationary cosmology. Unlike Λ, the dynamical field can support long wavelength fluctuations which leave an imprint on the CMB and the large scale distribution of matter. Another, critical distinction is that w, the ratio of the pressure (p) to the energy density (ρ), is $-1 < w \leq 0$ for quintessence, whereas w is precisely -1 for Λ. Hence, the expansion history of the Universe for Λ and Q models are different. There is much rich behavior to explore in a cosmological model with quintessence.

Furthermore, fundamental physics, *e.g.* those theories of gravity and fundamental interactions beyond the standard model of particle physics, provide motivation for light scalar fields (*e.g.* [10, 11, 12, 13]), one of which may serve as a cosmic Q field. In this way, quintessence serves as a bridge between the fundamental theory of nature, string theory or other, and the observable structure of the Universe.

The aim of this lecture is to present a survey of the quintessence cosmological scenario. The focus is on qualitative results, but detailed references are provided. Beginning with Sec. II, the observations leading to the missing energy problem and the claims of cosmic acceleration will be presented. Cosmology is currently a data driven enterprise, and it is startling to find that the observations are forcing theory to hypothesize the existence of a new energy component. In Sec. III, the cosmological constant is discussed as a possible solution. However a simple solution it provides, a Λ presents an enigma not understood by current theory. On the other hand, as argued in Sec. IV, experience with the tools commonly used to develop theories beyond the standard model of particle physics or Einstein's theory of gravitation leads us to propose the existence of a cosmic scalar field as a logical solution to the current problems in cosmology. The properties of quintessence and the quintessence plus cold dark matter (QCDM) scenario will also be presented in this section. Various species of quintessence, especially trackers, will be discussed in Sec. V. The observational constraints will be evaluated in Sec. VI, and the future outlook summarized in

Sec. VII.

II Observational Background

Current observational data are driving cosmology in new and unexpected directions, leading to the quintessence hypothesis. This hypothesis rests on three basic pieces of evidence.

First, the energy density in matter which clusters is well below the critical energy density required to close the Universe: $\Omega_m < 1$. This result has been developing over a number of years [1]. One way to illustrate this result is to consider the mass-to-light ratio on increasingly large length scales. At the scale of clusters and superclusters, the largest objects in the Universe, the mass-to-light ratio appears to turn over, reaching a value near M/L $\sim$ 200 [14]. By Oort's method, the matter density is $\Omega_m = (M/L)\times(j/\rho_{crit})$ where j is the observed luminosity density, obtaining $\Omega_m \sim 0.2 - 0.3$. Another method is to consider the baryon fraction in clusters, which is estimated to be $\Omega_b/\Omega_m \sim 0.1 - 0.2$ [15]. Then using the Big Bang Nucleosynthesis constraint $\Omega_b h^2 = 0.02$ [16] we obtain a similarly low value, $\Omega_m \sim 0.2 - 0.5$ for reasonable values of the hubble parameter, h.

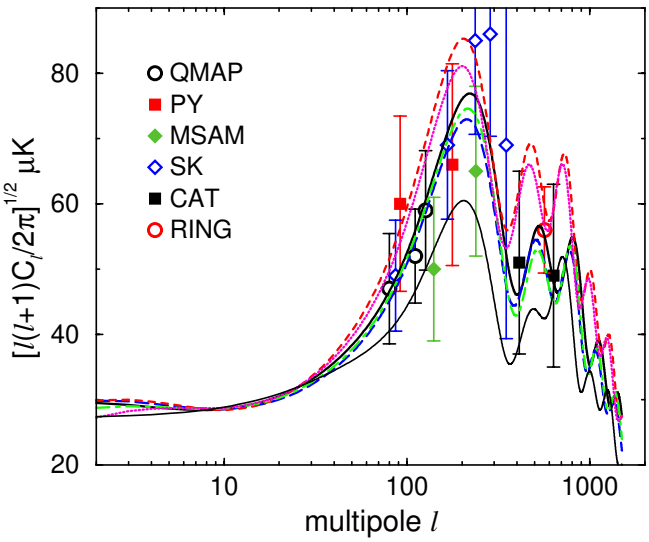

Figure 1. The conformal structure of the CMB is shown. The surface of the cone represents the flight path of photons traveling from the surface of last scattering. The dominant contribution to the temperature anisotropy is due to acoustic oscillations in the baryon-photon plasma on the scale of the sound horizon at recombination. Using the apparent size of this length scale in the CMB sky, the spatial curvature is determined to be small.

Second, the Universe is spatially flat. This has been argued on the basis of recent CMB results which show the presence of a sharp feature in the temperature anisotropy spectrum on the very angular scale predicted for a spatially flat Universe [17]. The way this works is straightforward. The predominant source of temperature anisotropy is through the Sachs-Wolfe effect, whereby photons climb out of deep gravitational potentials on the surface of last scattering, depicted in Fig. 1. At recombination, the deepest and largest length-scale gravitational potential into which photons can fall is limited by the sound horizon. The consequence is a sharp peak in the anisotropy spectrum on the angular scale corresponding to the apparent size of the sound horizon at recombination. As a problem in geometric optics, the relation between the angular scale and the size of the sound horizon depends on the spatial curvature and distance to the last scattering surface. The prediction is that the peak should occur at a multipole $\ell \approx 220/\sqrt{1-\Omega_k}$ where Ω_k is the spatial curvature expressed as a fraction of the critical energy density [18]. The location of the observed peak [3] as shown in Fig. 2 strongly supports the claim of a spatially flat Universe, with $|\Omega_k| \ll 1$.

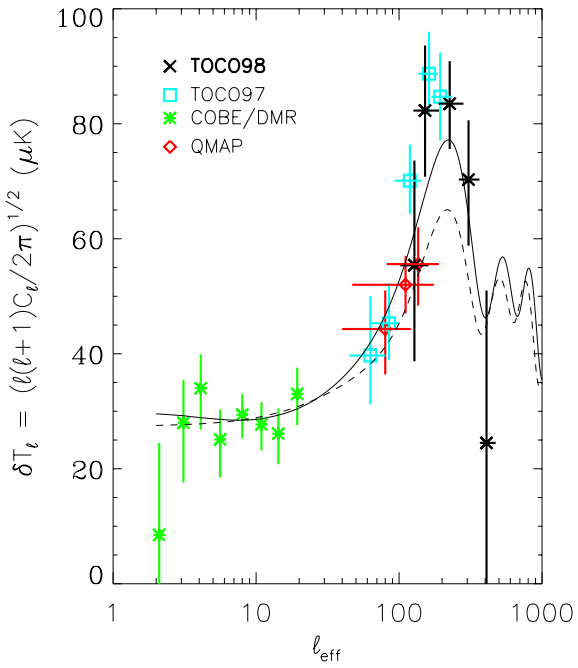

Figure 2. The angular power spectrum from COBE [19, 20], Saskatoon [21], QMAP [22], TOCO97 [23], and TOCO98 ([3] from which this figure is taken) are shown. The rise and fall in the anisotropy spectrum in the range $\ell \sim 100 - 300$ in the TOCO98 data is the strongest evidence to date that the spatial curvature of the Universe is small. The cosmological models are SCDM (dashed line: $\Omega_m = 1$, $\Omega_b = 0.05$, $h = 0.5$) and a Λ concordance model [24] (solid line: $\Omega_m = 0.33$, $\Omega_b = 0.041$, $\Omega_\Lambda = 0.67$, and $h = 0.65$.) The error bars are 1σ statistical.

The first two pieces of information alone are enough to argue for the existence of an additional energy component. Examining the FRW equations, which can be

rewritten as a sum rule for the fractional energy densities,

$$\begin{aligned} \frac{3}{8\pi G}H^2 &= -\frac{k}{a^2} + \sum \rho_i \\ 1 &= \Omega_k + \sum \Omega_i, \end{aligned}$$

we see that $\Omega_m < 1$ and $|\Omega_k| \ll 1$ indicate that there must be some other term, $\Omega_?$, which brings the total up to unity. There must be some other component which dominates the total energy density today. But wait — there's more.

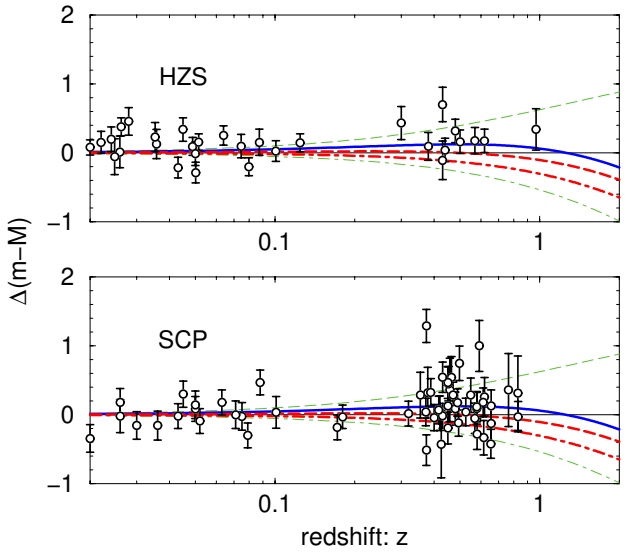

Figure 3. The magnitude - red shift relationship traced by the type 1a supernovae measured by the SCP [6] and HZS [7] groups is shown. The vertical axis shows the magnitude difference with respect to an open, empty (accelerating) Universe, represented by the curve $\Delta(m-M) = 0$. The top-most curve is the prediction for a $\Omega_\Lambda = 1$ model; the bottom-most curve is for a $\Omega_m = 1$ model. The weight of the data strongly rules out the $\Omega_m = 1$ Universe, and favors models with $\Omega_m = 0.3$ and $w = -1, -2/3, -1/3$ in decreasing order (the blue dashed, red dashed, and red dot-dashed curves).

Third, the cosmic expansion of the Universe is accelerating. This stunning claim is made on the basis of the magnitude - red shift relationship traced out by type 1a supernovae [6, 7], as shown in Fig. 3. The procedure can be summarized briefly. Although type 1a SNe are not standard candles, in that their intrinsic luminosity is not known, there appears to be an empirical relationship between the shape of the supernovae light curve and the luminosity. Hence, given the luminosity and the observed flux, the distance is determined; the red shift is determined by the host galaxy. The magnitude - red shift relationship then traces out an extended Hubble diagram, beyond the linear regime, which is sensitive to the cosmic acceleration. The evidence strongly favors a Universe in which the expansion is growing faster than that driven by pressureless dust. Since the acceleration of the expansion scale factor is

$$\ddot{a} = -a\frac{4\pi G}{3}(\rho + 3p),$$

the observations demand negative pressure to be provided by an additional component.

Putting these three pieces of evidence together, the intersection indicates a low density, spatially flat, accelerating Universe. The stage is set for the entrance of a dominant energy component with negative pressure.

III A Cosmological Constant?

Until a few years ago, when the CMB data began to crystallize and the SNe results were first reported, there was been no compelling reason to consider a spatially flat, low matter density, accelerating Universe. Indeed, theoretical prejudice favored simpler models, such as standard CDM with $\Omega_m = 1$ (for inflation enthusiasts) or open CDM. The cosmological constant was a curiosity, first introduced by Einstein in a failed attempt to obtain a static solution for a dust-filled Universe. However, the cosmological constant has come back into vogue as a popular candidate to fill the gap between the matter and critical density required for a flat Universe, and drive accelerated expansion with its negative pressure [25].

The shift of focus onto Λ has developed in response to the new observational data. Yet, introducing Λ revives several difficult questions [26]. If there is a cosmological term, a constant energy density and pressure, how did it arise? Is it a consequence of quantum gravity? Is it the self-gravitating energy associated with zero-point quantum fluctuations? Naive attempts to understand such a Λ typically associate it with zero-point quantum fluctuations, but require an ultraviolet cut-off, such as the energy scale of a symmetry breaking transition, to render it finite. Some quick numbers indicate the energy scale must be exceedingly low: $(H^2/G)^{1/4} \sim 10^{-3}$ eV. The problem of the hierarchy of energy scales in particle physics is exacerbated by this reasoning.

Consider the problem of the energy scale of Λ in another way. In order for the constant energy density to be dominant today, it must have been a negligible fraction of the total energy density of the Universe at all times in the past. It's difficult then to see how such an energy component could have ever been in equilibrium or contact with the rest of the cosmic fluid. As we will argue later, perhaps this component did not always have a constant, or nearly constant energy density.

By the principle of Occam's Razor, the simplest explanation for the missing energy component may be the cosmological constant. After all, there is just one number to specify, Λ itself. Occam's Razor, however, is not

a law of physics, and if too broadly applied it can obscure the interpretation of experiment. As we argue in the next section, a dynamical component is a logical candidate for the missing energy.

IV Quintessence: A Dynamical Component

The proposal of a cosmic scalar field, quintessence, strikes this author as the most logical way to model the missing energy, at present. The most basic tool employed to build a fundamental theory beyond the standard model of particle physics or Einstein gravity is the scalar field. The Higgs, inflaton, Brans-Dicke, moduli, and dilaton fields are examples of such scalar fields which play a critical role in models of fundamental physics. Furthermore, there is precedent to solving "missing energy" problems with a new particle or field, as was the case with the neutrino (a success) and dark matter (to be determined, but supersymmetric particles are strong candidates). In addition, the wide range of behavior encompassed by a scalar field provides a greater context in which to explore and understand the developing cosmological observations. In the limiting case of $w \to -1$, the quintessence field is indistinct from a Λ. As well, with a scalar field, it is simple to model the behavior of other forms of energy, such as a network of frustrated topological defects [27].

An important motivation for considering quintessence models is to address the "coincidence problem," the issue of explaining the initial conditions necessary to yield the near-coincidence of the densities of matter and quintessence today. For the case of Λ, as described earlier, the only possible option is to finely tune the ratio of energy densities to 1 part in $\sim 10^{110}$ at the end of inflation. Symmetry arguments from particle physics are sometimes invoked to explain why the cosmological constant should be zero [28] but there is no known explanation for a positive, observable vacuum density. For quintessence, because it can couple to other forms of energy either directly or gravitationally, one can envisage the possibility of interactions which cause the quintessence component to naturally adjust itself to be comparable to the matter density today. In fact, recent investigations [9, 29] have introduced the notion of "tracker field" models of quintessence which have attractor like solutions [30, 31] which produce the current quintessence energy density without the fine tuning of initial conditions. Particle physics theories with dynamical symmetry breaking or non-perturbative effects have been found which generate potentials with ultra-light masses which support negative pressure, and exhibit the "tracker" behavior [13, 32]. These suggestive results lend appeal to a particle physics basis for quintessence, as a logical alternative to an *ad hoc* invocation of a cosmological constant.

IV.1 The QCDM Scenario

The quintessence plus cold dark matter (QCDM) cosmological scenario is constructed as follows. The space-time is a spatially flat FRW with line element $ds^2 = a^2(-d\eta^2 + d\vec{x}^2)$. The cosmic fluid contains quintessence, CDM, plus all the standard model particles in the form of baryons, radiation, and neutrinos. The Universe evolves from an inflationary phase, during which time a spectrum of adiabatic density perturbations are generated, through radiation- and matter-dominated phases, until the present quintessence-dominated era.

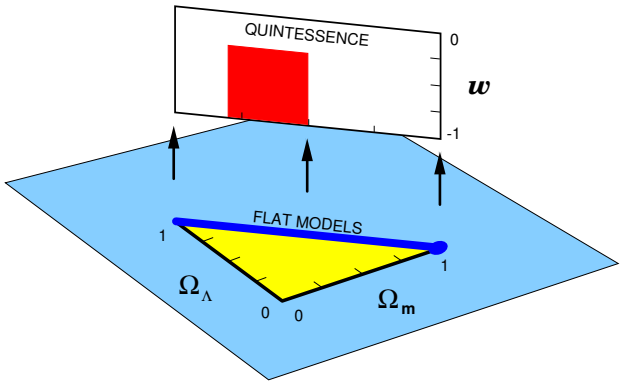

Figure 4. Quintessence introduces the equation of state, w, to the space of cosmological parameters. The most important quantities for characterizing a QCDM model is w and the matter density, $\Omega_m = 1 - \Omega_Q$.

IV.2 Background Evolution Equations

The evolution of a cosmic scalar field is obtained by the following set of equations. Starting from the Lagrangian for a self-interacting scalar field, the field is broken into a background, homogeneous portion Q and an inhomogeneous perturbation δQ. The equations of motion for the background field in an expanding FRW space-time are simply obtained:

$$L = \frac{1}{2}\partial_\mu Q \partial^\mu Q - V(Q) \quad \to \quad Q'' + 2\frac{a'}{a}Q' = -V_{,Q}.$$

Here, the prime indicates the derivatives with respect to conformal time. One need only specify a potential to evolve the equations and obtain the energy density and pressure,

$$\rho = \frac{1}{2}\dot{Q}^2 + V, \qquad p = \frac{1}{2}\dot{Q}^2 - V.$$

Hence, a potential energy dominated scalar field will give rise to an equation of state $w < 0$. An equivalent formulation of the scalar field is to specify the evolution

of the equation of state as a function of the scale factor, $w(a)$. Then the energy density can be reconstructed as

$$\rho(a) = \Omega_Q \rho_{crit} \exp\left(3\int_a^1 [1+w(a)]\, d\ln a\right),$$

and the pressure is simply $p = w\rho$. It is possible to reconstruct the potential and field evolution for a given equation of state [34, 33]:

$$\begin{aligned} V(a) &= \frac{1}{2}[1-w(a)]\rho(a) \\ Q(a) &= \int d\tilde{a}\frac{\sqrt{1+w(\tilde{a})}}{\tilde{a}H(\tilde{a})}\sqrt{\rho(\tilde{a})}. \end{aligned}$$

The equivalence $w(a) \leftrightarrow V(Q[a])$ immensely simplifies the simulation of quintessence.

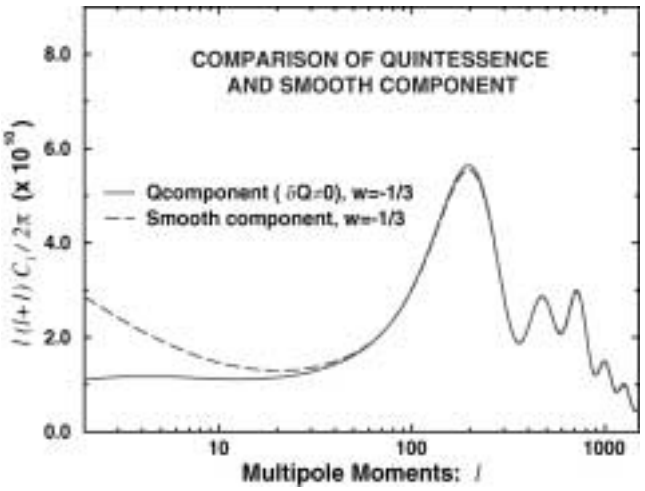

Figure 5. The fluctuations in quintessence are important on large scales. As a demonstration, the CMB anisotropy is computed for a smooth component, where δQ is artificially set to zero in a model with $\Omega_m = 0.3$ and $w = -1/3$; the fluctuations δQ which would normally cancel with the strong, late time integrated Sachs-Wolfe terms in the CMB, are absent, leading to a dramatically difference anisotropy spectrum. The fluctuations distinguish Q from Λ, and provide insight into the microphysical properties of Q.

IV. 3 Fluctuation Evolution Equations

The spatial fluctuations follow the evolution equation

$$\delta Q'' + 2\frac{a'}{a}\delta Q' + (V_{,QQ} - \nabla^2)\delta Q = -\frac{1}{2}h'Q'$$

where h is the trace of the synchronous gauge metric perturbation. (See [35] for details of the perturbation theory.) This equation is amenable to Fourier decomposition of the fluctuations. We see that the quintessence reacts to the external gravitational field of, say, dark matter and baryons through h. The nature of the response is determined by $V_{,QQ}$, which characterizes the effective mass, $m_Q = \sqrt{V_{,QQ}}$, or the Compton wavelength of the field, $\lambda_Q = 1/\sqrt{V_{,QQ}}$. Again there is a simplification using the equation of state:

$$\begin{aligned} a^2 V_{,QQ} = &-\frac{3}{2}(1-w)\left[\frac{a''}{a} - \left(\frac{a'}{a}\right)^2\left(\frac{7}{2}+\frac{3}{2}w\right)\right] \\ &+\frac{1}{1+w}\left[\frac{w'^2}{4(1+w)} - \frac{w''}{2} + w'\frac{a'}{a}(3w+2)\right] \end{aligned}$$

By making the change of variables to $\widetilde{\delta Q} = \delta Q/\sqrt{1+w}$ then the w'' term drops out of the evolution equation, so that w and w' need only be specified. We see that for a slowly varying equation of state, $|w'|/(1+w) \leq a'/a$, then $V_{,QQ} \propto H^2$ and the Compton wavelength of the quintessence field is approximately the Hubble horizon radius, $\lambda_Q \sim H^{-1}$. From the above equations, this means that fluctuations δQ on scales smaller than the Hubble scale dissipate, so the field is a smooth, non-clustering component there. Any initial fluctuations in the quintessence field are damped out rapidly. On scales greater than H^{-1}, the field is unstable to gravitational collapse, and long wavelength perturbations develop. This means the quintessence responds to the large scale fluctuations in the CDM and baryons. As shown in Fig. 5, the quintessence fluctuations play an important role in the large angle CMB anisotropy spectrum.

V Tracker Quintessence

Trackers represent a particular class of quintessence models which avoid the problem of fine tuning the initial conditions of the scalar field in order to obtain the desired energy density and equation of state at the present time [9, 29]. The tracker is a scalar field Q which rolls down a potential V(Q), as shown in Fig. 6, according to an attractor-like solution to the equations of motion. The solution is an attractor in the sense that a very wide range of initial conditions for Q and Q' rapidly approach a common evolutionary track, so that the cosmology is insensitive to the initial conditions. Tracking has an advantage similar to inflation in that a wide range of initial conditions is funneled into the same final condition. The initial energy density of the quintessence, $\rho_Q|_i$, can vary by nearly 100 orders of magnitude without altering the cosmic history. In particular, the acceptable initial conditions include equipartition after inflation — nearly equal energy density in Q as in the other 100 - 1000 degrees of freedom (*e.g.* $\Omega_Q|_i \approx 10^{-3}$). Furthermore, the cosmology has desirable properties. The equation of state of Q varies according to the equation of state of the dominant component of the cosmological fluid. As displayed in Fig. 7, when the Universe is radiation-dominated, then w is less than or equal to $1/3$ and ρ_Q decreases less rapidly than the radiation density. When the Universe is matter-dominated, the w is negative and ρ_Q decreases less rapidly than the matter density. The consequence is that eventually ρ_Q surpasses the matter density and

becomes the dominant component. At this point, the Hubble damping of the field evolution becomes important, Q slows to a crawl and $w \to -1$ as $\Omega_Q \to 1$ and the Universe is driven into an accelerating phase. The fact that Ω_Q is not seen to be completely dominating yet, or that Ω_m is measured to be at least 0.2, provides a natural lower bound to the tracker quintessence equation of state: $w \geq -0.8$.

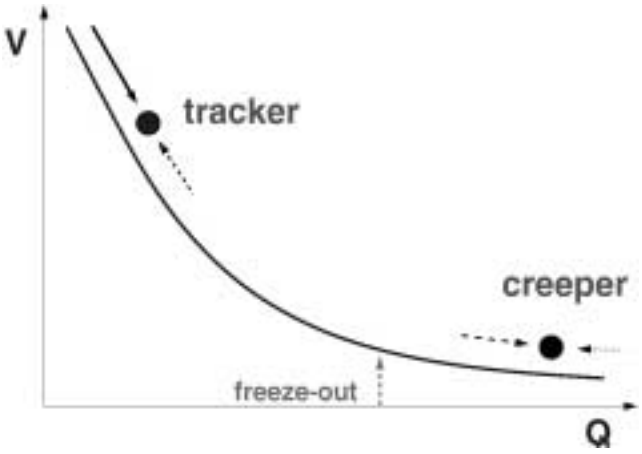

Figure 6. The characteristic shape of the potential for tracker and creeper quintessence models is shown; for these runaway scalar fields, the potential is high and steep at small Q and falls off, approaching zero as Q becomes large. Starting from a wide range of initial conditions, an interplay between the Hubble damping and the curvature of the potential drives the field evolution towards a common evolutionary track, in which the equation of state is always more negative than the background. Inevitably, the field comes to dominate the cosmological fluid, driving accelerated expansion. Once the field reaches the freeze-out point, the rolling field is critically damped by the Hubble expansion as $w \to -1$ and $\Omega_Q \to 1$.

Tracking occurs for any potential for which $w < w_B$, where w_B is the equation of state of the background fluid (*e.g.* radiation or matter), $\Gamma \equiv V''V/(V')^2 > 1$ and is nearly constant, $d(\Gamma - 1)/dt \ll (\Gamma - 1)H$. Once tracking begins, the equation of state is given by the handy formula

$$w \approx \frac{w_B - 2(\Gamma - 1)}{1 + 2(\Gamma - 1)}.$$

Two examples of tracking potentials are $V = M^4[\exp(M_{pl}/Q) - 1]$ where M_{pl} is the Planck mass, and $V = M^{4+\alpha}/Q^\alpha$ with $\alpha > 0$. For $\alpha = 1$, $\Gamma = 2$ which yields $w \approx (w_B - 2)/3 < w_B$ so that sooner or later the tracker will come to dominate. In each case, M is a free parameter which is fixed by the measured value of Ω_Q. Hence, these models each have one free parameter, just as for the cosmological constant. The tracker, however, has a much more plausible origin in particle physics, as the potentials occur in string and M-theory models associated with moduli fields or fermion condensates (perturbative effects make flat direction potentials runaway), and can start from a realistic state in equipartition. For these reasons the claim is made that quintessence is on equal if not stronger theoretical ground than the cosmological constant.

Another species of quintessence closely related to the tracker is the creeper. This corresponds to the case in which the initial energy density in Q after inflation is much greater than the radiation energy density. For either of the potentials described above, this corresponds to starting at a small value of Q, very high up in V. The consequent evolution is such that the field rapidly rolls down the potential, out to a very large value of the field, at $Q \sim M_{pl}$. The field evolution is critically damped; Q still moves, but is now creeping down the potential. As such, the equation of state is very nearly $w \approx -1$ and the creeper behaves very much like a cosmological constant.

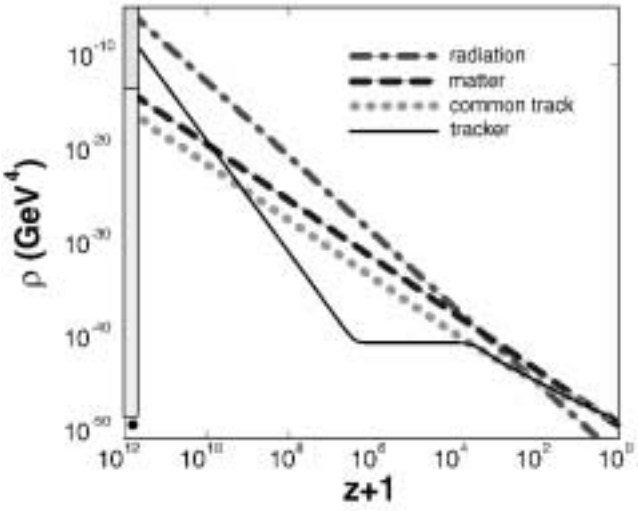

Figure 7. The energy density versus red shift for a tracker field is shown. Starting with initial conditions anywhere in the vertical box at left, including the yellow region which represents equipartition, to the singularly tuned black dot as required for Λ, the tracker field (black line) rapidly joins the common evolutionary track (orange dashed line). The tracker quintessence rapidly overtakes the radiation (red) and matter (blue) and comes to dominate the Universe by today. The red shift $z = 10^{12}$ has been arbitrarily chosen as the initial time. (Figure provided by [29].)

VI Concordance and Quintessence

We now focus on the observational constraints on QCDM cosmological models. These results were explored in depth in [24], where an exhaustive study of the constraints was presented, obtaining a set of quintessence models in concordance with observation.

The QCDM cosmological scenario can be characterized by the following five parameters: the quintessence equation of state w; the matter density parameter Ω_m, where a flat model is assumed so that $\Omega_m = 1 - \Omega_Q$; the baryon density parameter, Ω_b; the Hubble parameter, related to the Hubble constant by $H =$

$100\,h$ km/s/Mpc; the power law index of the spectrum of primordial density fluctuations in the matter and radiation,

n_s. In the case of tracker quintessence, the equation of state changes slowly with time, but the observational predictions are well approximated by treating w as a constant, equal to

$$\tilde{w} \approx \int da \Omega_Q(a) w(a) \; / \; \int da \Omega_Q(a).$$

Through out this discussion, we will evaluate the bounds for a constant w, but the same constraints hold for the equivalent QCDM model with $\tilde{w}$.

We now summarize the most important constraints, breaking them up by red shift.

VI.1 Low Redshift

Hubble Constant: The Hubble constant has been measured through numerous techniques over the years. Although there has been a marked increase in the precision of extragalactic distance measurements, the accurate determination of H has been slow. The H_0 Key Project [36], which aimed to measure the Hubble constant to an accuracy of 10%, currently finds $H = 73 \pm 6(\mathrm{stat}) \pm 8(\mathrm{sys})$km/s/Mpc; the method of type 1a supernovae gives $H = 63.1 \pm 3.4(\mathrm{internal}) \pm 2.9(\mathrm{external})$km/s/Mpc [37]; typical values obtained from gravitational lens systems are $H \sim 50 - 70$km/s/Mpc with up to $\sim 30\%$ errors [38, 39]. Other measures can be listed, but clearly convergence has not been reached, although some methods are more prone to systematic uncertainties. Based on these diverse measures, our conservative estimate for the Hubble constant is $H = 65 \pm 15$ km/s/Mpc with 2σ uncertainty.

Age of the Universe: Recent progress in the dating of globular clusters and the calibration of the cosmic distance ladder has relaxed the lower bound on the age of the Universe. We adopt $t_0 \geq 9.5$Gyr as a 95% lower limit [40, 41].

Baryon Density: Recent observations of the deuterium abundance by Burles and Tytler [16] yield $D/H = 3.4 \pm 0.3(\mathrm{stat}) \times 10^{-5}$. If this value reflects the primordial abundance, then Big Bang nucleosynthesis [42] with three light neutrinos gives $\Omega_b h^2 = 0.019 \pm 0.002$ where the 1σ error bars allow for possible systematic uncertainty.

Baryon Fraction: Observations of the gas in clusters have been used to estimate the baryon fraction (compared to the total mass) to be $f_{gas} = (0.06 \pm 0.003) h^{-3/2}$ [15]. The stellar fraction is estimated to be less than 20% of the gas fraction, so that $f_{stellar} = 0.2 h^{3/2} f_{gas}$. Next, simulations suggest that the baryon fraction in clusters is less than the cosmological value by about 10% [43] representing a depletion in the abundance of baryons in clusters by a fraction of 0.9 ± 0.1. Hence, the cosmological baryon fraction $f_b = (\Omega_b / \Omega_m)$ is estimated to be $f_b = (0.067 \pm 0.008) h^{-3/2} + 0.013$ at the 1σ level. Using the observed baryon density from BBN, we obtain the constraint

$$\Omega_m = \frac{0.019 h^{-2}}{0.067 h^{-3/2} + 0.013} \, (1 \pm 0.32)$$

at the 2σ level. For $h = 0.65$ this corresponds to a value of $\Omega_m = 0.32 \pm 0.1$.

σ_8: The abundance of x-ray clusters at $z = 0$ provides a model dependent normalization of the mass power spectrum at the canonical $8h^{-1}$Mpc scale. The interpretation of x-ray cluster data for the case of quintessence models has been carried out in detail by Wang and Steinhardt [44], in which case the constraint is expressed as

$$\begin{aligned} \sigma_8 \Omega_m^{\gamma} &= (0.5 - 0.1\Theta) \pm 0.1 \\ \gamma &= 0.21 - 0.22w + 0.33\Omega_m + 0.25\Theta \\ \Theta &= (n_s - 1) + (h - 0.65) \end{aligned}$$

where the error bars are 2σ. This fitting formula is valid for the range of parameters considered here.

Perhaps the two most important constraints on the mass power spectrum at this time are the COBE [19] limit on large scale power and the cluster abundance constraint which fixes the power on $8h^{-1}$ Mpc scales. Together, they fix the spectral index and leave little room to adjust the power spectrum to satisfy other tests.

VI.2 Intermediate Redshift

Supernovae: Type 1a supernovae are not standard candles, but empirical calibration of the light curve - luminosity relationship suggests that the objects can be used as distance indicators. There has been much progress in these observations recently, and there promises to be more. Hence, a definitive constraint based on these results would be premature. However, we examine the recent results of the High-Z Supernova Search Team (HZS: [7]) and the Supernova Cosmology Project (SCP: [6]) to constrain the luminosity distance - red shift relationship in quintessence cosmological models. We have adopted the following data analysis procedure: we use the supernova data for the shape of the luminosity - red shift relationship only, allowing the calibration, and therefore the Hubble constant, to float; we excise all SNe at $z < 0.02$ to avoid possible systematics due to local voids and overdensities; for SNe at $z > 0.02$, we assume a further uncertainty, added in quadrature, corresponding to a peculiar velocity of 300 km/s in order to devalue nearby SNe relative to the more distant ones (for the SCP data, a velocity of 300 km/s has already been included). There is substantial scatter in the supernovae data; the scatter is so wide that no model we have tested passes a χ^2 test with the full SCP data set; using a reduced set, Fit

C, argued in [6] as being more reliable, a finite range of models do pass the χ^2 test, comparable to the range obtained by the χ^2 test using the HZS data set. To gauge the current situation, we will report both χ^2 tests and maximum likelihood tests; to be conservative, we use the largest boundary (the χ^2 test based on HZS data using MLCS analysis) for our concordance constraint.

Lensing Statistics: The statistics of multiply imaged quasars, lensed by intervening galaxies or clusters, can be used to determine the luminosity distance - red shift relationship, and thereby constrain quintessence cosmological models. There exists a long literature of estimates of the lensing constraint on Λ models (*e.g.* spanning [45] to [46]). In one approach, the cumulative lensing probability for a sample of quasars is used to estimate the expected number of lenses and distribution of angular separations. Using the Hubble Space Telescope Snapshot Survey quasar sample [47] found four lenses in 502 sources, Maoz and Rix [48] arrived at the limit $\Omega_\Lambda \leq 0.7$ at the 95% CL. In a series of studies, similar constraints have been obtained using optical [49] and radio lenses [46]. Waga and collaborators [50, 51] have generalized these results, finding that the constraint weakens for larger values of the background equation of state, $w > -1$. In our evaluation of the constraint based on the HST-SSS data set, we find that the 95% confidence level region is approximately described by $\Omega_Q \leq 0.75 + (1+w)^2$, until the inequality is saturated at $w = -1/2$, consistent with the results of Waga. In principle, this test is a sensitive probe of the cosmology; however, it is susceptible to a number of systematic errors (for a discussion, see [52, 53]). Uncertainties in the luminosity function for source and lens, lens evolution, lensing cross section, and dust extinction for optical lenses, threaten to render the constraints compatible with or even favor a low density universe over $\Omega_m = 1$. Taking the above into consideration, none of the present constraints on quintessence due to the statistics of multiply imaged quasars are prohibitive: models in concordance with the low-z constraints are compatible with the lensing constraints.

VI.3 High Redshift

One of the most powerful cosmological probes is the CMB anisotropy, an imprint of the recombination epoch on the celestial sphere. The large angle temperature anisotropy pattern recorded by COBE [19] can be used to place two constraints on cosmological models.

COBE norm: The observed amplitude of the CMB power spectrum is used to constrain the amplitude of the underlying density perturbations. We adopt the method of Bunn and White [54] to normalize the power spectrum to COBE. As we use a modified version of CMBFAST [55] to compute the CMB anisotropy spectra, this normalization is carried out automatically.) We have verified that this method, originally developed for Λ and open CDM models, can be applied to the quintessence cosmological models considered in this work [34]. Of course, there is uncertainty associated with the COBE "normalization": the 2σ uncertainty in rms quantities is approximately 20% (see footnote #4 in [54]), which conservatively allows for statistical errors, as well as the systematic uncertainty associated with the differences in the galactic and ecliptic frame COBE map pixelizations, and potential contamination by high-latitude foregrounds [56].

n_s: COBE has been found to be consistent with a $n_s = 1.2 \pm 0.3$ spectral index [57, 58], but this assumes the only large angular scale anisotropy is generated via the Sachs-Wolfe effect on the last scattering surface. This neglects the baryon-photon acoustic oscillations, which produce a rise in the spectrum, slightly tilting the spectrum observed by COBE. In general, the spectral index determined by fitting the large angular scale CMB anisotropy of a quintessence model, which is also modified by a late-time integrated effect, to the shape of the spectrum tends to overestimate the spectral tilt. For example, analysis of a class of CDM models [59] (ΛCDM and SCDM, a subset of the models considered here) finds a spectral tilt $n_s = 1.1 \pm 0.1$. We conservatively restrict the spectral index of the primordial adiabatic density perturbation spectrum, with $P(k) \propto k^{n_s}$, to lie in the interval $n_s \in [0.8, 1.2]$. Note that inflation generically predicts $n_s \sim 1$, with n_s slightly less than unity preferred by inflaton potentials which naturally exit inflation.

Small Angle CMB: Dramatic advances in cosmology are expected in the near future, when the MAP and Planck satellites return high resolution maps of the CMB temperature and polarization anisotropy. When the measurements are analyzed, we can expect that the best determined cosmological quantities will be the high multipole C_ℓ moments, such that any proposed theory must first explain the observed anisotropy spectrum. At present, however, there is ample CMB data which can be used to constrain cosmological models.

We take a conservative approach in applying the small angular scale CMB data as a model constraint. Our intention is to simply determine which quintessence models are consistent with the ensemble of CMB experiments, rather than to determine the most likely or best fitting model. At the time of this lecture, the results from several experiments had either been recently presented or shortly expected, so that a detailed analysis would have been premature.

VI.4 Concordance Results

We have evaluated the cosmological constraints for the set of quintessence models occupying the five dimensional parameter space: w, Ω_m, Ω_b, h, n_s. The results are best represented by projecting the viable models onto the $\Omega_m - h$ and $\Omega_m - w$ planes.

The concordance region due to the suite of low red shift constraints, including the COBE normalization and tilt n_s, are displayed in Figs. 8, 9. Each point in the shaded region represents at least one model in the remaining three dimensional parameter space which satisfies the observational constraints.

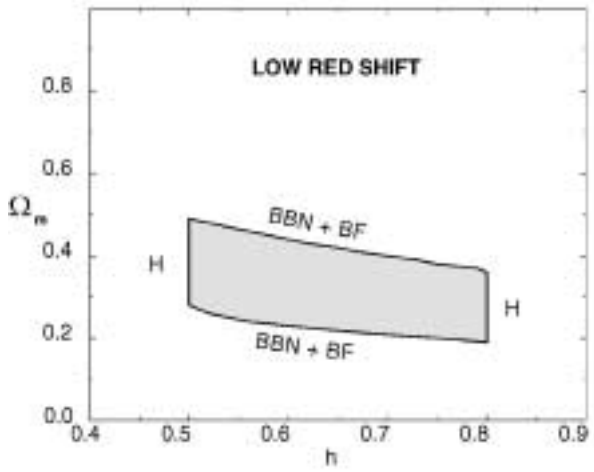

Figure 8. The projection of the concordance region on the $\Omega_m - h$ plane, on the basis of the low red shift observational constraints only, is shown. The observations which dominate the location of the boundary are labeled.

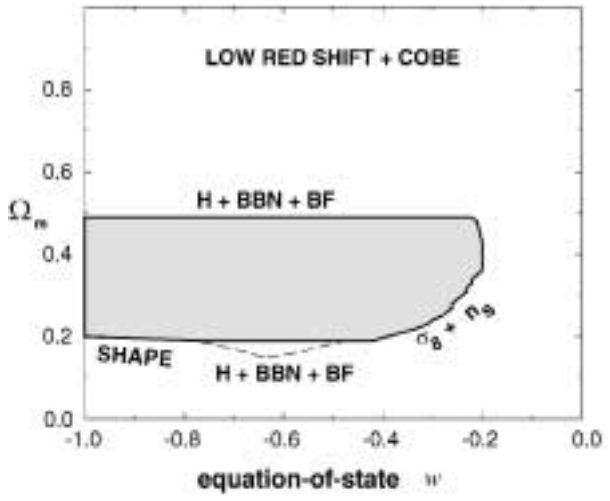

Figure 9. The projection of the concordance region on the $\Omega_m - w$ plane, on the basis of the low red shift and COBE observational constraints only, is shown. The observations which dominate the location of the boundary are labelled. If a wider range for the baryon density is allowed, such as $0.006 < \Omega_b h^2 < 0.022$, the shape of the mass power spectrum (not discussed here: see [24]) and σ_8 constraint determine the location of the low Ω_m boundary, and the concordance region extends slightly as shown by the light dashed line.

In Fig. 8, the boundaries in the Ω_m direction are determined by the combined BBN and BF constraints as a function of h, while h is only restricted by our conservative allowed range and the age constraint. The age does not impact the $\Omega_m - h$ concordance region, since for the allowed values of Ω_m and h, there is always a model with a sufficiently negative value of w to satisfy the age constraint. Relaxing either the BBN or BF constraint would raise the upper limit on the matter density parameter to allow larger values of Ω_m. This requires a simultaneous reduction in the spectral index, n_s, in order to satisfy both the COBE normalization and cluster abundance.

In Fig. 9, the upper and lower bounds on Ω_m are again determined by the combination of BBN, BF, and h. The lower bound on Ω_m due to the combination of the BBN and BF constraints can be relaxed if we allow a more conservative range for the baryon density, such as $0.006 < \Omega_b h^2 < 0.022$ [60, 61]. However, the constraints due to σ_8 and the shape of the mass power spectrum take up the slack, and the lower boundary of the concordance region is relatively unaffected. The lower bound on Ω_m near $w = -1$ is determined in part by the shape of the mass power spectrum (see [24]); the mass power spectrum in a model with low Ω_m and strongly negative w is a poor fit to the shape of the APM data, based on a χ^2-test. This constraint on models near $w = -1$ is relaxed if we allow anti-bias ($b < 1$), although $b < 1$ is strongly disfavored on a theoretical basis. At the other end, for $w \geq -0.6$, the lower bound on Ω_m is determined by the combination of the upper bound on the spectral index, and the x-ray cluster abundance constraint on σ_8. If we further restrict the bias to $b < 1.5$, a small group of models at the upper right corner with $w \geq -0.2$ and $\Omega_m \geq 0.4$ will fail the shape test.

We see that models occupying the fraction of the parameter space in the range $-1 \leq w \leq -0.2$ and $0.2 \leq \Omega_m \leq 0.5$ are in concordance with the basic suite of observations, suggesting a low density universe. It is important to note that the set of viable models spans a wide range in w; the concordance region is not clustered around $w = -1$, or Λ, but allow such diverse behavior as $w \sim -1/3$. However, the case $w = 0$, which can result from the scaling exponential potential [30, 31] is clearly in contradiction with observation: the Ω_m required by the x-ray cluster abundance constraint is incompatible with the matter density parameter allowed by the BF and BBN constraints. Hence, the models with $w = 0$ explored by Ferreira and Joyce [62] are not viable.

The most potent of the intermediate red shift constraints is due to type 1a supernovae, which we present in Fig. 10. In addition to the SCP results, the HZS group has presented two different analyses of their catalog of SNe, based on multi-color light curve shapes

(MLCS) and template fitting; hence we show three SNe results. Carrying out a maximum likelihood analysis, all three give approximately the same result for the location of the 2σ bound, favoring concordant models with low Ω_m, and very negative w. Based on a maximum likelihood analysis SCP have reported a limit $w \leq -0.6$ at the 1σ level. A χ^2 analysis of the same data gives a somewhat different result: the Fit C SCP data and the HZS data sets give comparable, although weaker, results to the likelihood analysis. In the spirit of conservativism, we have used the weakest bound which we can reasonably justify. Hence, for the concordance analysis, we use the 2σ contour resulting from a χ^2 test.

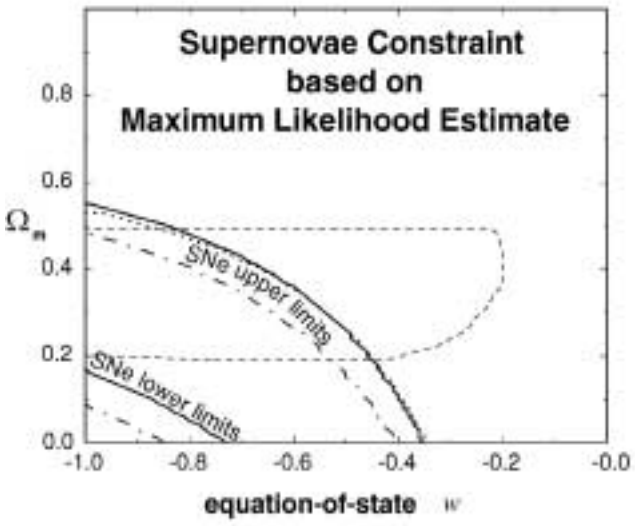

Figure 10. The 2σ maximum likelihood constraints on the $\Omega_m - w$ plane, due to the SCP (solid), HZS MLCS (short dashed), and HZS template fitting methods (dot-dashed). The light, dashed line shows the low red shift concordance region.

We have evaluated the high red shift constraint due to the select ensemble of CMB anisotropy measurements. Based on a χ^2 test in δT_l, the set of concordant models projected down to the $\Omega_m - h$ and $\Omega_m - w$ planes is unchanged from the low red shift concordance region at even the 1σ level. This "null" result from the CMB should not be too surprising; the current observational data is capable only of discerning a rise and fall in power in the C_ℓ spectrum across $\ell \sim 100 - 300$. The results are unchanged if we include additional current CMB results, or use a χ^2 test in $\ln(\delta T_l^2)$ [63]. Rather, we must wait for near-future experiments which have greater $\ell-$coverage, *e.g.* BOOMERANG, MAT, and MAXIMA, which are expected to significantly reduce the uncertainties.

Since the submission of this manuscript, the data from the MAT [3] (see Fig. 2) and BOOMERANG [64] experiments have been released. However, neither significantly changes our results.

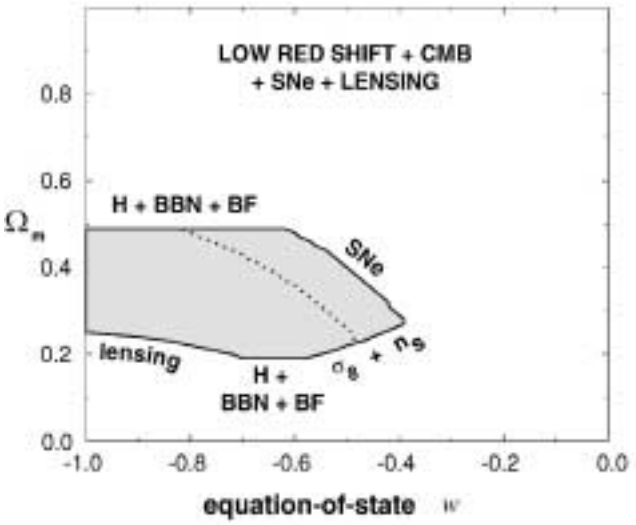

Figure 11. The dark shaded region is the projection of the concordance region on the $\Omega_m - w$ plane with the low, intermediate, and high red shift observational constraints. The dashed curve shows the 2σ boundary as evaluated using maximum likelihood, which is the same as Fig. 10.

Thus far we have applied the low red shift constraints in sequence with one of the other intermediate or high red shift constraints. It is straight forward to see how the combined set of constraints restrict the quintessence parameter space. Taking the low red shift constraint region, which is shaped primarily by the BF, BBN, H, and σ_8 constraints, the dominant bounds on the $\Omega_m - w$ plane are then due to SNe and lensing. The SNe drives the concordance region towards small Ω_m and negative w; the lensing restricts low values of Ω_m. Putting these all together, an ultimate concordance test is presented in Fig. 11. If the present observations are reliable, we may conclude that these models are the most viable among the class of cosmological scenarios considered herein.

To what degree do current uncertainties in the Hubble parameter, the spectral tilt and other cosmic parameters obstruct the resolution in w? To judge this issue, we have performed an exercise in which we fix $h = 0.65$, $\Omega_b h^2 = 0.019$, and we choose the spectral tilt to insure that the central values of the COBE normalization and the cluster abundance constraint are precisely satisfied. In Figs. 12 and 13, we show how different constraints restrict the parameter planes. Note first the long, white concordance region that remains in the $\Omega_m - w$ plane, which is only modestly shrunken compared to the concordance region obtained when current observational errors are included. The region encompasses both Λ and a substantial range of quintessence. Hence, current uncertainties in other parameters are not critical to the uncertainty in w. The figure further shows how

each individual constraint acts to rule out regions of the plane. The color or numbers in each patch represent the number of constraints violated by models in that patch. It is clear that regions far from the concordance region are ruled out by many constraints. Both figures also show that the boundaries due to the constraints tend to run parallel to the boundary of the concordance region. Hence, shifts in the values or the uncertainties in these measurements are unlikely to resolve the uncertainty in w by ruling out one side or the other — either the constraints will remain as they are, in which case the entire concordance region is allowed, or the constraints will shift to rule out the entire region.

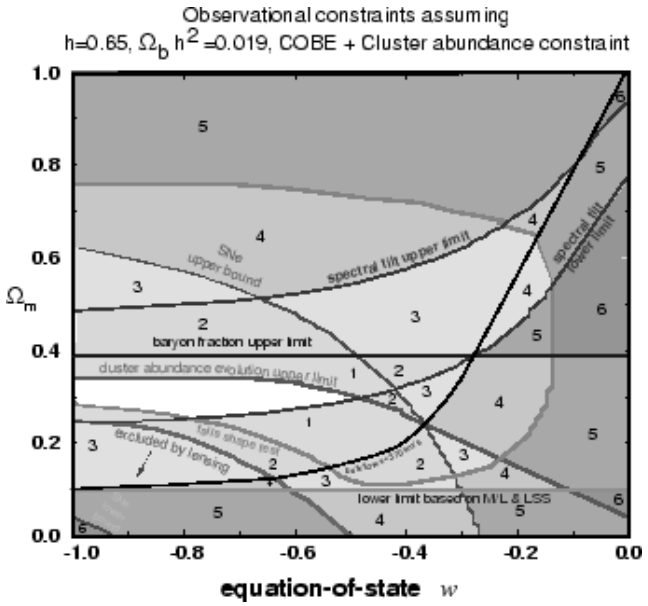

Figure 12. The concordance region (white) resulting if we artificially set $\Omega_b h^2 = 0.019$ and fix the spectral tilt to precisely match the central values of COBE normalization and cluster abundance measurements. The curves represent the constraints imposed by individual measurements. The curves divide the plane into patches which have been numbered (and colored) according to the number of constraints violated by models in that patch.

The tracker models are a particularly important class of quintessence models, as discussed earlier, because they avoid the ultra-fine tuning of initial conditions required by models with a cosmological constant or other (non-tracking) quintessence models. An additional important feature of these models is that they predict a definite relationship between the present day energy density and pressure, which yields a lower bound on the constant, effective equation of state, near $\widetilde{w} \sim -0.75$ [29]. Note that the effective or averaged equation of state as described earlier is about 10 per cent larger than the value of w today. In Fig. 14 we add this bound to the low red shift constraints, obtaining the concordance region for tracker quintessence. This region retains the core of our earlier low red shift concordance, and is consistent with the SNe constraints. A creeper field has an equation of state $w = -1$, marked in Figs. 14, and is effectively indistinguishable from a cosmological constant today.

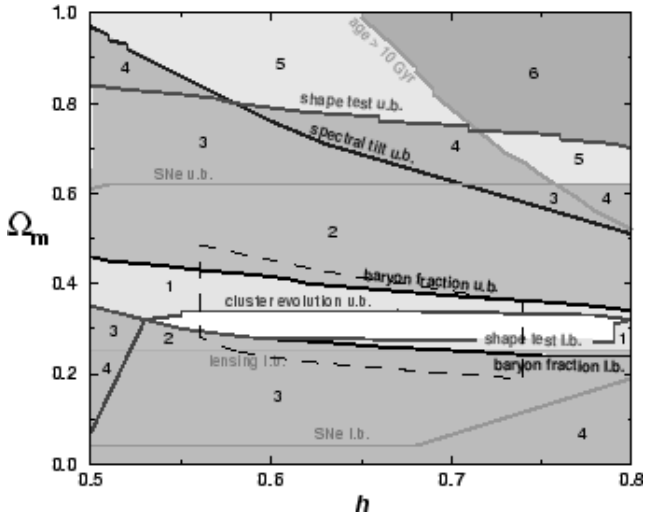

Figure 13. The concordance region (white) resulting if we artificially set $h = 0.65$ and $\Omega_b h^2 = 0.019$ precisely and fix the spectral tilt to precisely match the central values of COBE normalization and cluster abundance measurements. The curves represent the constraints imposed by individual measurements. The curves divide the plane into patches which have been numbered (and colored) according to the number of constraints violated by models in that patch.

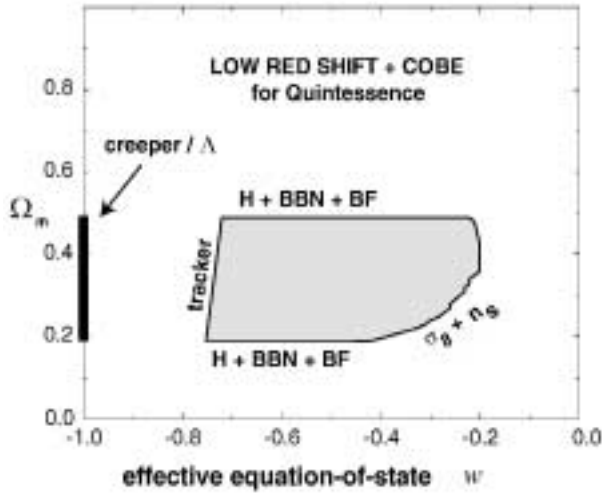

Figure 14. The concordance region based on COBE and low red shift tests for tracker quintessence is shown. The thin black swath along $w = -1$ shows the allowed region for creeper quintessence and Λ. The equation-of-state is time-varying; the abscissa is the effective (average) w.

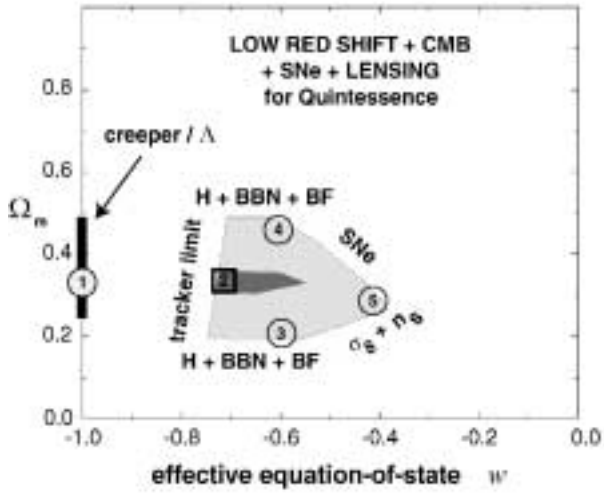

Figure 15. The overall concordance region based low, intermediate, and high red shift tests for tracker quintessence is shown. The thin black swath along $w = -1$ shows the allowed region for creeper quintessence and Λ. The equation of state is time-varying; the abscissa is the effective (average) w. The dark shaded region corresponds to the most preferred region (the 2σ maximum likelihood region consistent with the tracker constraint), $\Omega_m \approx 0.33 \pm 0.05$, effective equation-of-state $w \approx -0.65 \pm 0.10$ and $h = 0.65 \pm 0.10$ and are consistent with spectral index $n = 1$. The numbers refer to the representative models that appear in Table I of [24] and that are referenced frequently in the text. Model 1 is the best fit ΛCDM model and Model 2 is the best fit QCDM model.

In Fig. 15 we combine all current observations on tracker models. Since these are arguably the best-motivated theoretically, we identify from this restricted region a sampling of representative models with the most attractive region for quintessence models being $\Omega_m \approx 0.33 \pm 0.05$, effective equation of state $w \approx -0.65 \pm 0.07$ and $h = 0.65 \pm 0.10$ and are consistent with spectral index $n_s = 1$ indicated by the dark shaded region in Fig. 15. These models represent the best targets for future analysis. The challenge is to prove or disprove the efficacy of these models and, if proven, to discriminate among them.

VII Future Tests

The current observational data appear to indicate very unusual, interesting phenomena. If this trend continues, as more experiments measure the CMB, large scale structure, and the like, we will then find the evidence supporting new, very low energy physics. In the following, I have constructed an outline of a logical progression for experiments.

VII.1 Refine the Basic Parameters

The first order of business is to refine the measurements of the basic cosmological parameters. That is, we must verify that the matter density is low, $\Omega_m < 1$, that the spatial curvature is negligible, $|\Omega_k| \ll 1$, and that there is a missing energy problem. The measurement of the Hubble constant must also be further refined.

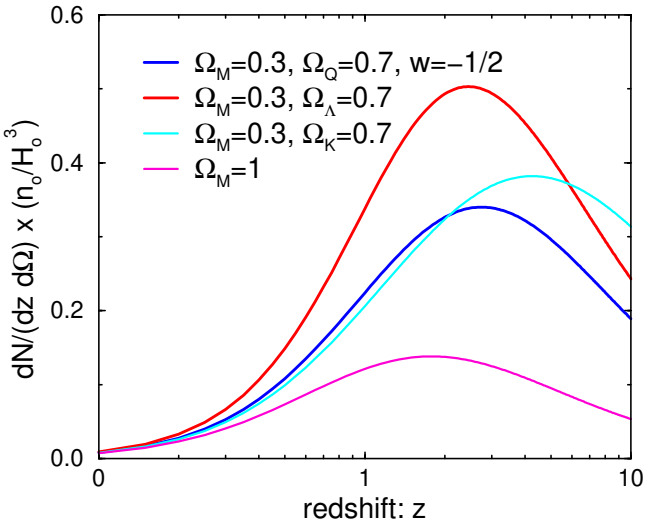

Figure 16. The differential volume - red shift relationship for a series of models is shown. The DEEP survey [65] will measure the differential volume out to $z \sim 1$. Given that the Universe is spatially flat, this test will be able to pin down the equation of state, w.

The experiments most likely to accomplish these goals in the near future are: MAP, which will measure the CMB and extract information about $\Omega_m h^2$, $\Omega_b h^2$, and n_s; the wide field surveys of large scale structure by the SDSS and 2dF, and the small field x-ray probes by Chandra and XMM, combined will reveal information about the large scale distribution of matter, giving insight into Ω_m; strong gravitational lensing systems and S-Z clusters will help pin down the value of h. These results will be in hand within several years, and should the missing energy problem persist, there will be a number of exciting ideas to test.

VII.2 Determine the Cosmic Evolution

Given that the missing energy problem is real, the next logical step will be to characterize the equation of state, measuring w and $\dot{w}$, to determine whether the dark energy is Λ, Q, or other. For fundamental physics, Λ or Q represents new, ultra-low energy phenomena beyond the standard model. If firmly established by observations, the discovery will go down in history as one of the greatest clues to the ultimate theory. The fact that the dark energy can be probed observationally is an unimaginable gift, since most unified theories entail ultra-high energies, far beyond laboratory access.

A test of the tracker quintessence scenario can be made by determining the change in the equation of state. If the equation of state can be measured at the present and at an earlier epoch, say $z \sim 1$, we can obtain a crude measure of the slope, dw/dt. Trackers have

the special property that the equation of state becomes more negative at late times: $w \to -1$ as $\Omega_Q \to 1$. A measurement of $dw/dt > 0$ would argue against tracker quintessence.

Probes of cosmic evolution are the most direct way to determine w. Hence, observations of the magnitude - red shift relationship using type 1a supernovae are ideal. The ongoing efforts of the SCP and HZS groups should improve the SNe constraints on w, if the understanding of systematic effects and the theoretical modeling of type 1a SNe improve. Another approach is to use the volume - red shift relationship, as with the rate of strong gravitational lensing or number counts. The Deep Extragalactic Evolutionary Probe [65] should be able to pin down w to 1% by studying the evolution of the apparent numbers of dark matter halos as a function of their circular velocity, provided selection effects are well controlled and Ω_m, Ω_Q are known.

VII.3 Determine the Microphysics

Once the basic properties of the dark energy are determined, Ω_Q and w, we can begin to ask questions about the microphysics — what is it? What clues can it reveal about the structure of the Universe and the nature of physical laws? Long wavelength fluctuations, manifest in very large scale structure and the CMB, are the clues to the microphysics of quintessence.

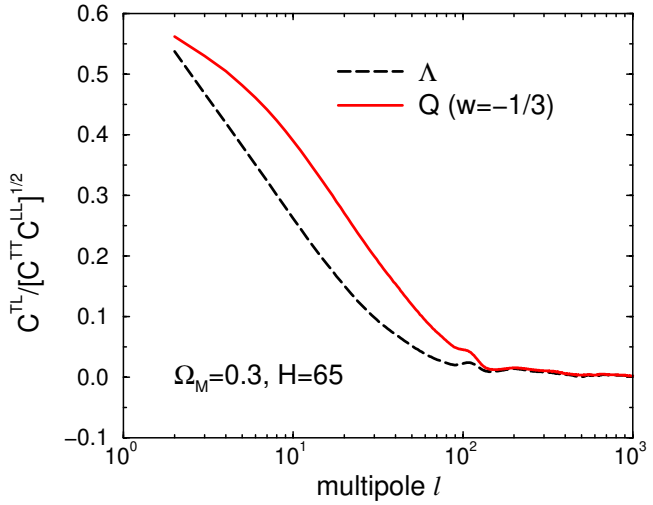

Figure 17. The cross-correlation of the CMB temperature anisotropy with the weak lensing convergence of the temperature field. The difference between the signals for a Λ and Q model, as shown, gives clues to the behavior of the gravitational potential at late times and on the largest scales.

The best approach in this case is to make full sky maps that trace cosmic structure on the largest scales. These maps can be cross-correlated to isolate the late time, large scale features unique to quintessence. Although cosmic variance blurs information on large length scales, cross-correlation can sharpen the picture. Taking the CMB for example, a given multipole moment can only be measured to $C_\ell \pm C_\ell/\sqrt{2\ell+1}$ due to cosmic variance, and at low ℓ the uncertainty is worse. However, cross correlation can dramatically reduce this uncertainty. Consider the cross-correlation coefficient between two fields on the sky, such as CMB temperature anisotropy and the x-ray background, or the weak lensing convergence of the temperature field [66, 67]. When the cross-correlation is strong, when $(C_\ell^{AB})^2 \sim C_\ell^{AA} C_\ell^{BB}$, then the cosmic variance is dramatically reduced, even on large angular scales, even for the quadrupole. Hence, a strong cross-correlation is probably the best tool to pin down the microphysics of the quintessence.

VII.4 Test the Framework

The missing energy problem and the quintessence hypothesis, and most current cosmological models, are predicated on the validity of Einstein's general relativity, and the existence of cold dark matter with a spectrum of adiabatic perturbations generated by inflation. At the same time that an effort is directed towards measuring cosmic parameters, it is necessary to test that GR is valid on the largest scales, and to probe for long range forces associated with the missing energy component. By testing the framework we can hope to make connections to fundamental physics.

Detection of a time or spatial variation in coupling constants, such as α or G, would indicate dramatically new physics. In models of fundamental physics, such as M-theory, these field couplings in four dimensions often appear as moduli fields describing the evolution of higher dimensions. Hence, a measurement of $\dot{G}$, say, would reinforce quintessential ideas of a dynamical, inhomogeneous energy component.

If the quintessence field is coupled to the Ricci scalar, there will be observable consequences if Q is rolling sufficiently fast. The constraints on scalar-tensor theories of gravity apply, and the cosmic evolution and long wavelength fluctuations will differ from the standard QCDM scenario. (For recent work, see [68, 69, 70]).

If the quintessence field is coupled to the pseudoscalar $F_{\mu\nu}\tilde{F}^{\mu\nu}$ of electromagnetism as suggested by some effective field theory considerations [71], the polarization vector of a propagating photon will rotate by an angle $\Delta\theta$ that is proportional to the change of the field value ΔQ along the path. CMB polarization maps can potentially measure the $\Delta\theta$ from red shift ~ 1100 to now [72] and distant radio galaxies and quasars can provide information of $\Delta\theta$ from red shift a few to now [71]. If these two observations generate non-zero results, they can provide unique tests for quintessence and the tracker hypothesis, because tracker fields start rolling early (say, before matter-radiation equality) whereas most non-tracking quintessence fields start rolling just recently (at red shift of a few).

The prospects for decisively testing the quintessence hypothesis in the immediate future are excellent. Whether these ideas are vindicated or not, we will surely discover exciting, new physics.

References

[1] V. Trimble, ARA&A **25**, 423 (1987).

[2] R. G. Carlberg *et al.*, ApJ **462**, 32 (1996).

[3] A. D. Miller *et al.*, ApJ **542**, L1 (1999).

[4] L. M. Krauss and M. S. Turner, Gen. Rel. Grav. **27**, 1137 (1995).

[5] J. P. Ostriker and P. J. Steinhardt, Nature **377**, 600 (1995).

[6] S. Perlmutter *et al.*, ApJ **517**, 565 (1998).

[7] A. G. Riess *et al.*, AJ **116**, 109 (1998).

[8] R. R. Caldwell, R. Dave, and P. J. Steinhardt, PRL **80**, 1582 (1998).

[9] I. Zlatev, L. Wang, and P. J. Steinhardt, PRL **82**, 896 (1998).

[10] I. Affleck *et al.*, Nucl. Phys. B **256**, 557 (1985).

[11] C. Hill and G. G. Ross, Nucl. Phys. B **311**, 253 (1988).

[12] P. Binetruy, M. K. Gaillard, and Y.-Y. Wu, Nucl. Phys. **B481**, 109 (1996).

[13] A. Masiero, M. Pietroni, and F. Rosati, Phys. Rev. D **61** 023504 (2000).

[14] N. A. Bahcall, L. M. Lubin, and V. Dorman, ApJ **447** L81 (1995).

[15] A. E. Evrard, MNRAS **292**, 289 (1997).

[16] S. Burles and D. Tytler, ApJ **507**, 732 (1997).

[17] L. Knox and L. Page, astro-ph/0002162 (2000).

[18] M. Kamionkowski, D. N. Spergel, N. Sugiyama, ApJ **426**, L57 (1994).

[19] C. L. Bennett *et al.*, ApJ **464**, L1 (1996).

[20] M. Tegmark, Phys. Rev. D **55**, 5895 (1997).

[21] C. B. Netterfield, M. J. Devlin, N. Jarosik, L. Page, and E. J. Wollack, ApJ **474**, 47 (1997).

[22] M. J. Devlin, A. de Oliveira-Costa, T. Herbig, A. D. Miller, C. B. Netterfield, L. Page, and M. Tegmark, ApJ **509**, L73 (1998).

[23] E. Torbet, M. J. Devlin, W. Dorwart, T. Herbig, M. R. Nolta, A. D. Miller, L. Page, J. Puchalla, and H. Tran, ApJ **521** L79 (1999).

[24] L. Wang, R. R. Caldwell, J. P. Ostriker, and P. J. Steinhardt, astro-ph/9901388 (1999).

[25] N. Bahcall, J. P. Ostriker, S. Perlmutter, and P. J. Steinhardt, Science **284**, 1481 (1999).

[26] S. Weinberg, Rev. Mod. Phys. **61**, 1 (1989).

[27] D. N. Spergel and U.-L. Pen, ApJ **491**, L67 (1996).

[28] T. Banks, hep-th/9601151 (1996).

[29] P. J. Steinhardt, L. Wang, and I. Zlatev, Phys. Rev. D **59**, 123504 (1999).

[30] B. Ratra and P. J. E. Peebles, Phys. Rev. D **37**, 3406 (1988).

[31] P. J. E. Peebles and B. Ratra, ApJ **325** L17 (1988).

[32] P. Binetruy, Phys. Rev. D **60**, 063502 (1999).

[33] R. R. Caldwell and P. J. Steinhardt, in *Proceeding of the Non-Sleeping Universe Conference*, ed. by T. Lago and A. Blanchard (Kluwer Academic, 1998).

[34] R. Dave, PhD. Thesis, University of Pennsylvania (1998).

[35] C.-P. Ma and E. Bertschinger, ApJ **455**, 7 (1995).

[36] W. L. Freedman *et al.*, in IAU Symp. 183, Cosmological Parameters and the Evolution of the Universe, ed. K. Sato, astro-ph/9801080, (1998).

[37] M. Hamuy *et al.*, AJ **112**, 2398 (1996).

[38] E. E. Falco *et al.*, ApJ **484**, 70 (1997).

[39] P. L. Schechter *et al.*, ApJ **475**, L85 (1997).

[40] B. Chaboyer *et al.*, ApJ **494**, 96 (1998).

[41] M. Salaris and A. Weiss, A & A **335**, 943 (1998).

[42] D. N. Schramm and M. S. Turner, Rev. Mod. Phys. **70**, 303 (1998).

[43] L. Lubin *et al.*, ApJ **460**, 10 (1996).

[44] L. Wang and P. J. Steinhardt, ApJ **508**, 483 (1998).

[45] E. L. Turner, J. P. Ostriker, and J. R. Gott III, ApJ **284**, 1 (1984).

[46] E. E. Falco, C. S. Kochanek, and J. A. Munoz, ApJ **494**, 47 (1998).

[47] D. Maoz *et al.*, ApJ **409**, 28 (1993).

[48] D. Maoz and H.-W. Rix, ApJ **416**, 425 (1993).

[49] C. S. Kochanek, ApJ **453**, 545 (1995); ApJ **466**, 638 (1996).

[50] L. F. Bloomfield-Torres and I. Waga, MNRAS **279**, 712 (1996).

[51] I. Waga and A. P. M. R. Miceli, Phys. Rev. D **59**, 1035 (1999).

[52] S. Malhotra, J. Rhoads, and E. Turner, MNRAS **288**, 138 (1997).

[53] Y.-C. Cheng and L. M. Krauss, ApJ **514**, 25 (1999).

[54] E. F. Bunn and M. White, ApJ **480**, 6 (1997).

[55] U. Seljak and M. Zaldarriaga, ApJ **469**, 437 (1996).

[56] K. M. Gorski *et al.*, ApJ **114**, 1 (1998).

[57] K. M. Gorski *et al.*, ApJ **464**, L11 (1996).

[58] G. Hinshaw *et al.*, ApJ **464** L25 (1996).

[59] S. Hancock *et al.* MNRAS **294**, L1 (1998).

[60] S. Levshakov, astro-ph/9808295 (1998).

[61] K. Olive, G. Steigman, and T. Walker, astro-ph/9905320 (1999).

[62] P. G. Ferreira and M. Joyce, Phys. Rev. Lett. **79**, 4740 (1997); Phys. Rev. D **58**, 023503 (1998).

[63] J. R. Bond, A. H. Jaffe, and L. Knox, astro-ph/9808264 (1998).

[64] P. D. Mauskopf *et al.*, astro-ph/9911444 (1999).

[65] J. A. Newman and M. Davis, astro-ph/9912366 (1999).

[66] U. Seljak and M. Zaldarriaga, astro-ph/9811123 (1998).

[67] H. Peiris and D. N. Spergel, astro-ph/0001393 (2000).

[68] L. Amendola, astro-ph/9906073, 9908023 (1999).

[69] F. Perrotta, C. Baccigalupi, S. Matarrese, Phys. Rev. D **61**, 023507 (2000).

[70] L. Parker and A. Raval, gr-qc/9908013, 9908069 (1999).

[71] S. Carroll, Phys. Rev. Lett. **81**, 3067 (1998).

[72] A. Lue, L. Wang, and M. Kamionkowski, Phys. Rev. Lett. **83**, 1506 (1999).